Available online at www.sciencedirect.com

jmr&t Journal of Materials Research and Technology

www.jmrt.com.br

Original Article

Structural and magnetic properties of $MgFe_2O_4$ powders synthesized by solution combustion method: the effect of fuel type

*P. Heidari, S.M. Masoudpanah**

School of Metallurgy & Materials Engineering, Iran University of Science and Technology (IUST), Tehran, Iran

ARTICLE INFO

Article history:
Received 1 February 2020
Accepted 20 February 2020
Available online 6 March 2020

Keywords:
$MgFe_2O_4$
Solution combustion synthesis
Fuel type
Magnetic properties

ABSTRACT

Single phase $MgFe_2O_4$ powders were synthesized by solution combustion method using metal nitrates as oxidant and ethylenediaminetetraacetic acid (EDTA), citric acid and glycine as fuel. Thermal analysis showed the combustion reaction rate decreased from the glycine to citric acid and EDTA fuel, respectively, due to the chelation of cations by fuel. The structural analysis of X-ray diffraction patterns showed the partially inverse spinel structure of $MgFe_2O_4$ powders in which the inversion degree was dependent on the fuel type. The particle size decreased from 250 to 45 and 35 nm for the glycine to the citric acid and EDTA fuels, respectively, as a result of the decrease of combustion temperature. The $MgFe_2O_4$ powders synthesized by the EDTA fuel had the highest specific surface area and pore volume of 62 m^2/g and 0.14 cm^3/g. The magnetic properties were correlated to the inversion degree and particle size.

1. Introduction

Combustion synthesis is a famous method for production of many functional and structural materials such as oxides, carbides, cements, etc. due to its simplicity, versatility and low-cost [1,2]. The combustion synthesis is based on a self-propagating exothermic reaction in which the released heat is sufficient for proceeding of the reaction [3]. The precursors are firstly mixed and then heated up to the ignition temperature via conduction, induction, microwave and laser heating method [4]. The initial precursors are usually solid powders (~1 μm), inducing the inhomogeneous combustion reaction. As a result, the following calcination and leaching treatments can be required for obtaining the final pure products. This challenge can be solved by using the initial soluble precursors in a proper solvent, benefiting the atomic-scale mixing of precursors [5].

Solution combustion synthesis (SCS) commonly utilizes the soluble precursors such as metal nitrates, chlorides, carbonates, etc., as oxidants and organic fuels such as urea, glycine, citric acid, etc., which are dissolved in water. The precursor solution is initially dried and then ignited by heating up [6,7]. The exothermic reaction occurs by burning or oxidation of organic fuels to CO_2, N_2 and H_2O gases. The liberated gases break down the large particles and form a plenty of pores. Therefore, the SCSed spongy products with high specific surface areas are appropriate for energy conversion and storage, catalysts, sensors, etc. [8,9]. The pore shape, size and volume and specific surface areas of SCSed products are mainly controlled by fuel type and contents, adjusting

* *Corresponding author.*
E-mail: masoodpanah@iust.ac.ir (S. Masoudpanah).
https://doi.org/10.1016/j.jmrt.2020.02.073

the combustion temperature and amount of released gases [10]. Although the high combustion temperature is required for synthesis of multicomponent compounds, but the specific surface areas decrease at high synthesis temperatures by particle growth and sintering [11]. Accordingly, the liberation of a large amount of gases increase the specific surface area, while the outgoing gases cool down the combustion product [12–14]. Furthermore, the characteristics of fuels such as molecular structure, functional groups, decomposition temperature, etc., effect on the combustion feature such as combustion reaction rate, combustion temperature, etc., [15]. The organic fuels can simultaneously chelate the various cations which is benefited for the chemical homogeneity in synthesis of the complicated compounds such as superconductors, spinels, perovskites, etc. [16–19].

In this work, the roles of fuel type (glycine, citric acid and ethylenediaminetetraacetic acid (EDTA)) on the physicochemical properties of magnesium ferrite ($MgFe_2O_4$) powders were explored. $MgFe_2O_4$ as a magnetic spinel ferrite has many suitable chemical and physical properties such as moderate saturation magnetization, high electrical resistance, low dielectric loss, and high chemical stability, inspiring many applications in drug delivery, hyperthermia, magnetic coils, antenna, gas sensors, etc. [20–24].

2. Experimental procedure

3 mmol of $Mg(NO_3)_2.6H_2O$ and 6 mmol of $Fe(NO_3)_3.9H_2O$ were firstly dissolved in 30 mL distilled water. Then, 9 mmol of fuel was added. The glycine ($C_2H_5NO_2$), citric acid ($C_6H_8O_7$) and EDTA ($C_{10}H_{16}N_2O_8$) were used as fuel. The precursor solution was dried by heating at 80 °C. The dried precursor was ignited by increasing temperature up to 250 °C. The combusted powders were hand-crashed by a pestle.

The combustion reaction rate was thermally analyzed by thermogravimetric analysis (TGA) and differential thermal analysis (DTA) on a STA BäHR 503 instrument. The air atmosphere and heating rate of 10 °C/min were used.

An X-ray powder diffractometer (PANalytical) system was used for collecting the diffraction patterns of the synthesized powders. The XRD patterns were recorded with the help of CuK_α radiation generated at 40 kV and 30 mA. The XRD patterns were also refined by Reitveld method using Xpert HighScore plus software for calculating the crystallite size and cation distribution. The particle shape and size were photographed by scanning (TESCAN Vega II) and transmission (Philips CM200) electron microscopies. A PHS-1020 instrument was used for measuring the N2 adsorption-desorption isotherms following the degassing of the powders at 250 °C for 5 h. The specific surface areas and pore volume were calculated from the adsorption isotherm by means of Brunauer–Emmett–Teller (BET) and Barrett–Joyner–Halenda (BJH) methods, respectively.

The magnetic properties of the powders were measured at room temperature using a vibrating sample magnetometer (Meghnatis Kavir Kashan Co., Iran).

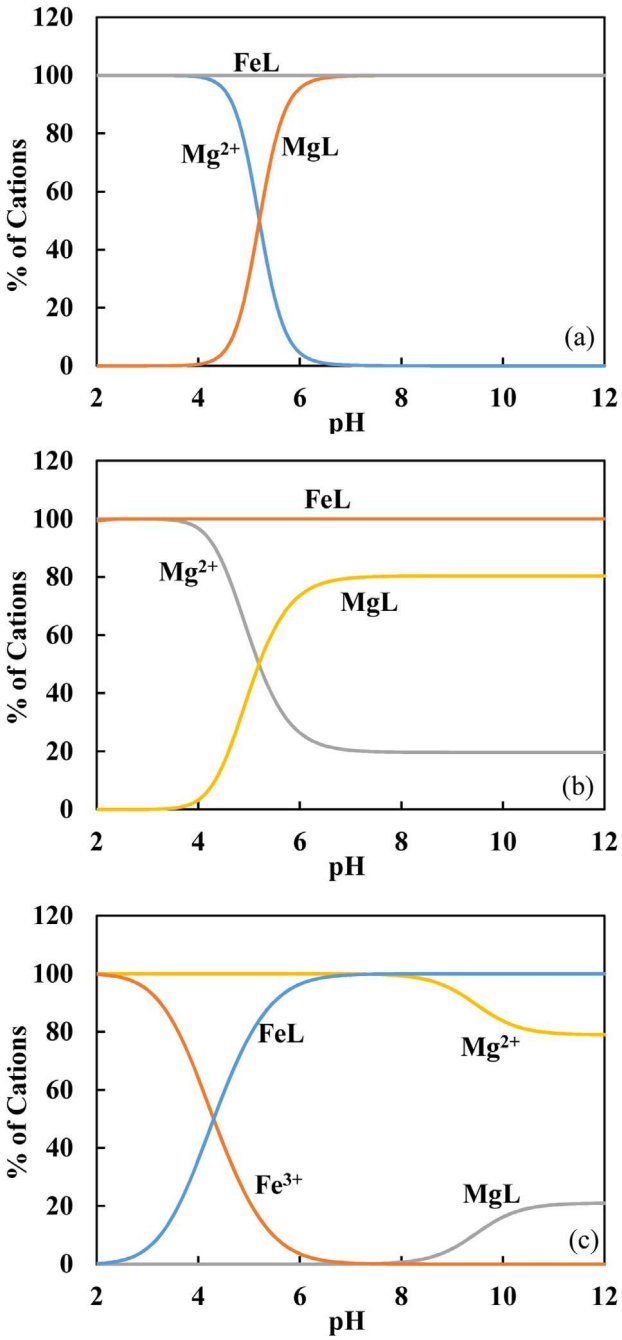

Fig. 1 – The distribution of cations as free cations and chelated species in the presence of (a) EDTA, (b) citric acid and (c) glycine (L shows the corresponding ligand).

3. Results and discussion

The organic fuels can effectively chelate the various cations via their amino (NH_2) and carboxylate (COO^-) groups. The chelated species can be connected together by the esterification process to form the long polymeric chains. Therefore, the cations are not separately precipitated during the gela-

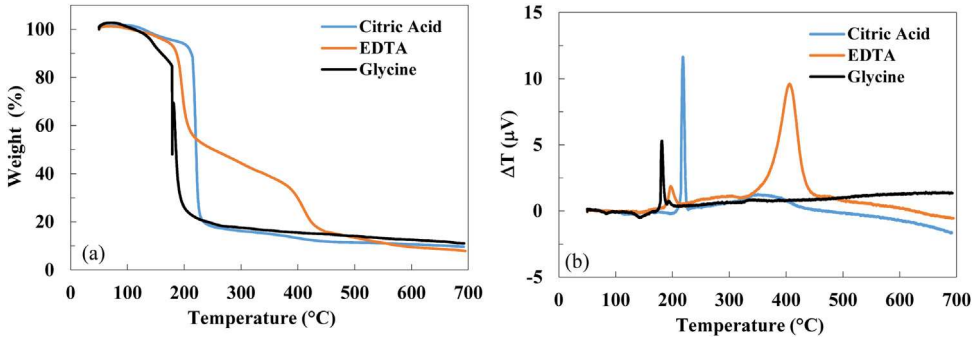

Fig. 2 – (a) TGA and (b) DTA curves of the dried gels.

tion process, leading to the chemical homogeneity [25]. The chelatability of fuels mainly depends on the amount of fuel and pH of precursor solution, as presented in Fig. 1. The molar ratio of fuel to total metal cations was considered as 1. EDTA is a weak acid with the molecular structure of $(COOHCH_2)_2N(CH_2)_2N(COOHCH_2)_2$) which the four end carboxylic acid groups can be completely ionized at pH ≥ 7. Furthermore, the two nitrogen atoms have unshared electron pairs and can participate in the formation of stable complexes [26]. Fig. 1a shows the stable complex with Fe^{3+} can be formed at all pH values, while the complete chelation of Mg^{2+} occurs at pH > 7. About 80 % of Mg^{2+} cations is complexed by the citric acid at pH ≥ 7 (Fig. 1b), due to its lower stability constants ($Log\beta_{11}$ = 3.27) in comparison with the EDTA ($Log\beta_{11}$ = 8.65). The citric acid ($COOHCH_2COHCOOHCH_2COOH$) has three carboxylic acid groups which can lose its protons by neutralization [27]. The ferric (Fe^{3+}) cations are completely chelated by citric acid. For the glycine fuel, almost of Mg^{2+} cations are free in the precursor solution, while all ferric cations are complexed at pH above 7. The low affinity of glycine molecule (NH_2CH_2COOH) toward the Mg^{2+} cations ($Log\beta_{11}$ = 1.98) can be attributed to the low polarizability and large cation size [28–30].

Thermal analysis curves of the various dried gels are presented in Fig. 2. The combustion exothermic reaction usually starts at low temperatures and is accompanied by a sharp weight loss due to the generation of gaseous products. The glycine fuel ignites at 180 °C with the weight loss of 65 %. Moreover, there is no more weight loss at the higher temperatures, indicating the complete combustion reaction. The combustion reaction occurs at the higher temperature of 220 °C with a higher weight loss (70 %) by using the citric acid fuel. The EDTA fuel combusts in two separately steps at the temperatures of 190 and 410 °C with the total weight loss of 80 %. The weak combustion reaction by EDTA is due to the chelation of cations with the carboxylic groups, while the amino groups of glycine intensify the combustion reaction rate [31]. Therefore, there is a compromise between the chelatability of fuel and combustion rate in which the chelation of cations by organic fuels decreases the combustion reaction rate.

The purity, crystal structure, crystallinity, crystallite size and lattice parameter of the MgFe2O4 powders can be obtained from the XRD patterns presented in Fig. 3. All diffraction peaks are indexed according to the spinel ferrite phase with the space group of F3dm. Therefore, single phase $MgFe_2O_4$ pow-

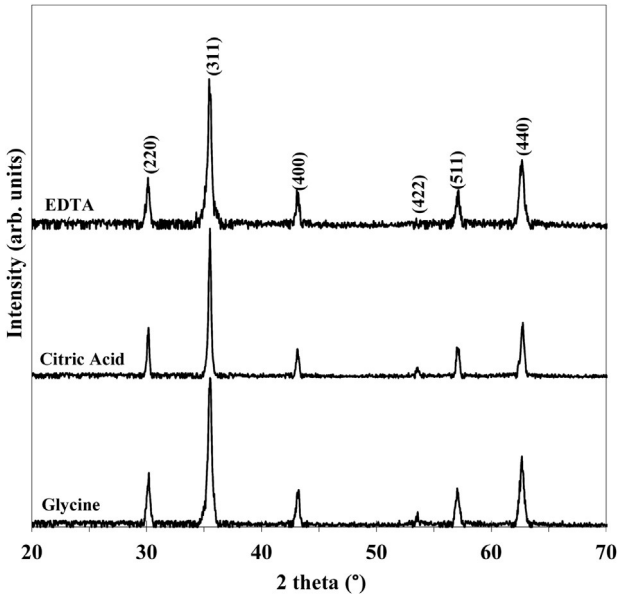

Fig. 3 – XRD patterns of the as-combusted powders as a function of fuel type.

ders are formed following the combustion reaction without further treatment. The directly formation of $MgFe_2O_4$ phase is due to the chemical homogeneity and liberation of enough thermal energy. The chelation of cations by fuel hinders the precipitation of hydroxides and subsequent segregation of oxides during combustion process. However, the high combustion temperature and high reaction rate can compensate the segregations for the direct formation of $MgFe_2O_4$ phase. In spite of the weak chelation by glycine fuel, the combusted powders are single phase magnesium ferrites due to its high combustion rate and temperature, it is vice versa for EDTA fuel. The structural properties such as lattice parameter, crystallite size and cation distribution are given in Table 1 as a function of fuel contents. The citric acid fuel results in the small lattice parameter compatible with the bulk value (a = 0.8387 nm [32]), indicating the high crystallinity of $MgFe_2O_4$ powders. However, the crystal defects in $MgFe_2O_4$ powders synthesized by the glycine and EDTA fuels are reasons for the difference between their lattice parameter and bulk value. The smallest value of crystallite size is for the EDTA fuel, while the high

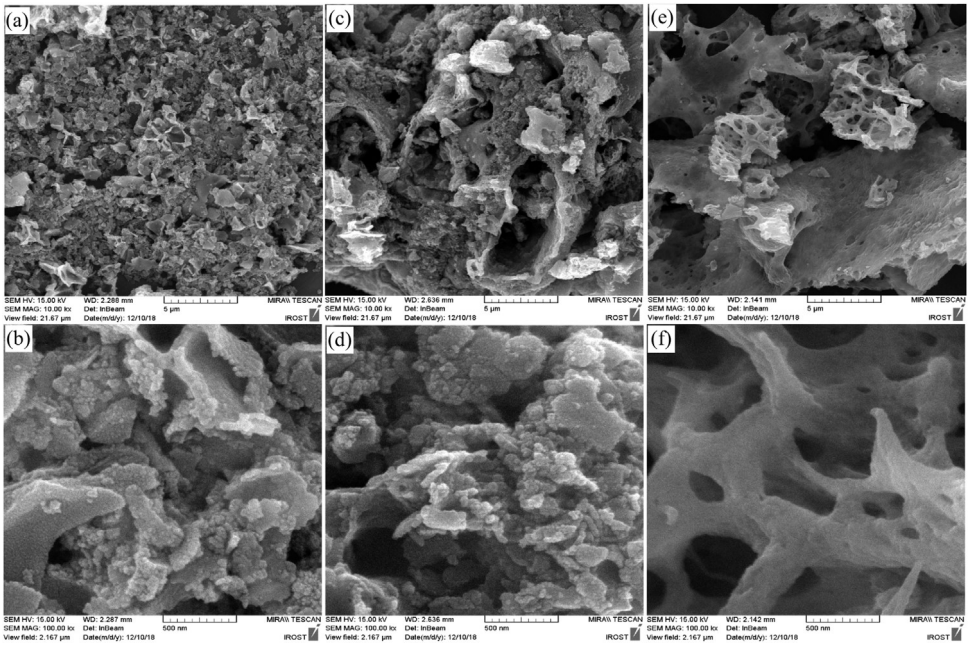

Fig. 4 – SEM images of the as-combusted $MgFe_2O_4$ powders by (a and b) EDTA, (c and d) citric acid, and (e and f) glycine fuels.

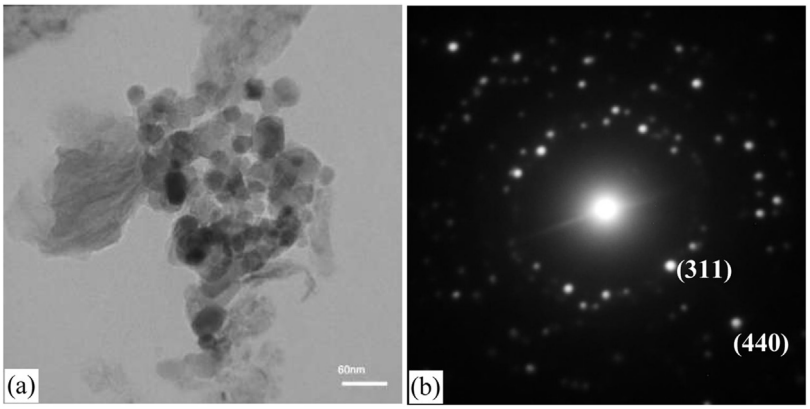

Fig. 5 – (a) TEM image and (b) SAED pattern of the MgFe2O4 powders obtained by the citric acid fuel.

Table 1 – Dependence of crystallite size, DXRD, lattice parameter, a, inversion degree, d, and cation distribution on fuel type.

Fuel	DXRD (nm)	a (nm)	δ	Cation distribution
EDTA	35	0.8356	0.943	$(Mg_{0.057}Fe_{0.943})_A[Mg_{0.943}Fe_{1.057}]_BO_4$
Citric Acid	41	0.8367	0.905	$(Mg_{0.095}Fe_{0.905})_A[Mg_{0.905}Fe_{1.095}]_BO_4$
Glycine	57	0.8377	0.873	$(Mg_{0.127}Fe_{0.873})_A[Mg_{0.873}Fe_{1.127}]_BO_4$

combustion temperature by the glycine fuel leads to grow of the $MgFe_2O_4$ crystallites.

The $MgFe_2O_4$ phase has the spinel structure in which the O^{2-} anions are arranged in cubic close packing and the Mg^{2+} and Fe^{3+} cations are distributed between the tetrahedral (A) and octahedral [B] sites. The cation distribution can be quantified using inversion degree (δ), as the fraction of Fe3+ cations in the tetrahedral sites, $(Mg_{1-\delta}Fe_{\delta})_A[Mg_{\delta}Fe_{2-\delta}]_BO_4$, which is mainly dependent on the site preferences of cations in terms of the size, covalent bonding effects and crystal field stabilization energies [33–35]. Since Fe^{3+}, being a d^5 ion, has no crystal field stabilization energy in an octahedral site, Fe^{3+} can be distributed over both the tetrahedral and octahedral sites; hence, the large Mg^{2+} cations preferentially occupy the octahedral [B] sites [32]. However, the inversion degree depends on the thermal history, especially the rate of cooling from high temperature following synthesis in which the quenched $MgFe_2O_4$ powders have a lower degree of inversion than slowly cooled powders [36]. Accordingly, the lower degree for glycine fuel is due to the high combustion temperature and then high cooling rate, while the lower combustion temperature by the EDTA fuel results in the higher inversion degree.

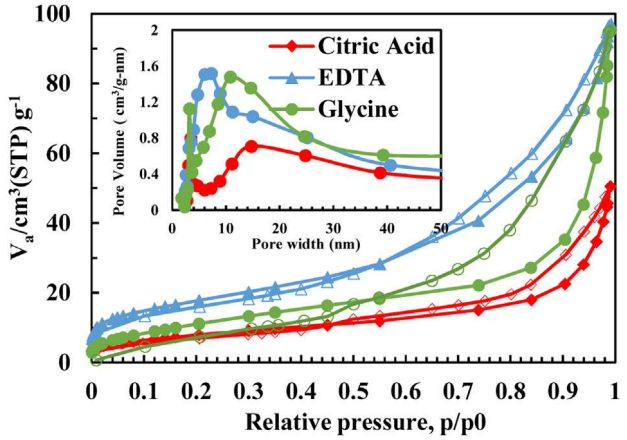

Fig. 6 – N2 adsorption (filled symbols) and desorption (open symbols) isotherms of the MgFe2O4 powders synthesized by various fuels.

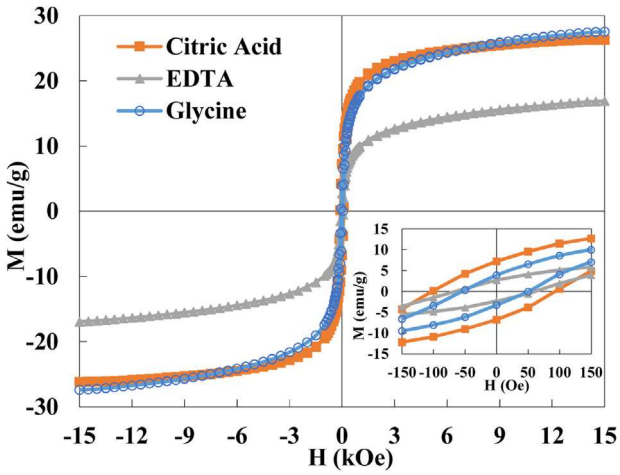

Fig. 7 – Magnetization curves of $MgFe_2O_4$ powders prepared by citric acid, glycine and EDTA fuels.

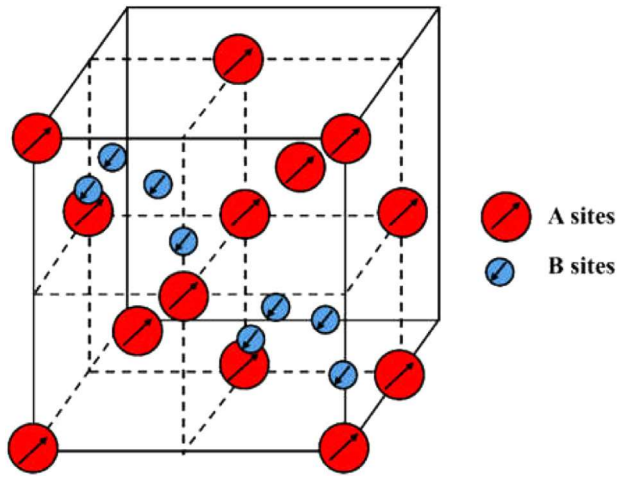

Fig. 8 – Magnetic structure of spinel ferrites. Only cations in the front four octants of the unit cell are shown. The antiparallel spins on A and B sites form alternate layers perpendicular to [111].

The morphology and microstructure of the as-combusted powders are strongly related to the fuel type and amount, as shown in Fig. 4. The average particle size decreases from 250 nm for glycine fuel to 45 and 35 nm for citric acid and EDTA fuels, respectively, due to the decrease of temperature and rate of combustion reaction. For the glycine fuel, the high combustion temperature is benefit for sintering and growth of particles, while their high amount of large pores can be attributed to the high combustion rate for generation of gaseous products. The uniform distribution of pore size by EDTA fuel is consequence of the low combustion reaction rate. TEM image and SAED pattern of the $MgFe_2O_4$ powders obtained by the citric acid fuel are given in Fig. 5. The cubic system of spinel $MgFe_2O_4$ is responsible for the formation of square-like particles [37,38]. The dot SAED pattern confirms the spinel structure and single crystal nature of particles.

The specific surface areas and pore size and shape can be concluded from the adsorption-desorption isotherms presented in Fig. 6. The isotherms are type IV which has the limiting uptake over a range of high relative pressure (p/p°). Moreover, the H3 hysteresis loop, due to the capillary condensation in mesopore structures, is related to the loosely assemblage of particles [39]. The BET specific surface area of $MgFe_2O_4$ powders is 62, 28 and 43 m^2/g for the EDTA, citric acid and glycine fuels, respectively. The high specific surface area for the EDTA fuel is as a result of the low combustion temperature, preventing from the particle sintering and growth. Although the glycine fuel has the high combustion temperature which decreases the specific surface area, but its highest reaction rate is benefit to release a large amount of gases, cooling the combustion products and breaking down the particles [7]. The pore size distribution plots are presented in the inset of Fig. 6. The powders have the mesopores in the range of 2–50 nm and micropores in the range of 1–2 nm. The pore volume decreases form 0.14 cm^3/g for the EDTA fuel to 0.13 and 0.07 cm^3/g for the glycine and citric acid fuels, respectively.

The magnetization curves of $MgFe_2O_4$ powders as a function of fuel type are given in Fig. 7. The saturation magnetization increases from 17 emu/g for the EDTA fuel to 26 and 27 emu/g for the citric acid and glycine fuels, respectively. The saturation magnetization (Ms) of spinel ferrites are strongly dependent on the cation distribution between tetrahedral and octahedral sites, because the magnetic spins of cations on tetrahedral (A) sites are antiparallel to those on octahedral [B] sites [40]. The contents of half of the unit cell are schematically shown in Fig. 8 in which the origin coincides on an A cation and oxide anions are not shown. The unit cell can be described as an fcc array of A cations, at corner and face center positions, with additional A cations in the center of alternate octants of the unit cell. The B cations are arranged tetrahedrally inside the other four octants [41,42]. The magnetic spins of A and B ions are antiparallel, as shown. Therefore, the magnetic moment per formula unit in μ_B (Bohr magneton) can be calculated by the following equation [43]:

$$n_B = M_B(x) - M_A(x) \quad (1)$$

which M_A and M_B are the net magnetic moments of A and B sites, respectively. The ionic magnetic moment of Fe^{3+} and

Mg^{2+} cations is considered as 5 and 0 μ_B, respectively. The higher difference of magnetic moment between A and B sites as in the low inversion degree case, the higher saturation magnetization. Accordingly, the lowest M_s by the EDTA fuel is related to the higher inversion degree and weak crystallinity.

The coercivity (H_c) values of powders are 100, 51 and 48 Oe for the citric acid, glycine and EDTA fuels, respectively. The coercivity is a strongly function of the particle size which it increases from zero up to a maximum and then decreases with the increase of particle size due to the formation of multidomain at large particle size instead of single domain [44]. Therefore, the low coercivity for the EDTA fuel is due to its very small particle size, while it is vice versa for the glycine fuel. The highest coercivity by the citric acid fuel is due to its optimum particle size and highest crystallinity.

4. Conclusions

Solution combustion synthesis method was used for preparation of single phase $MgFe_2O_4$ powders by means of various fuel type. The EDTA and citric acid fuels chelated both Mg^{2+} and Fe^{3+} cations at high pH values completely, while the glycine fuel cannot form the stable complexes with Mg^{2+} cations. The slow combustion reaction rate and low combustion temperature using EDTA fuel resulted in the highest inversion degree and smallest particle size. Moreover, the burning of EDTA fuel was benefited to obtain the high specific surface area due to the liberation of a large amount of gases. The $MgFe_2O_4$ powders synthesized by the glycine fuel had the saturation magnetization of 27 emu/g which was correlated to the low inversion degree.

Conflicts of interest

The authors declare no conflicts of interest.

REFERENCES

[1] Nersisyan HH, Lee JH, Ding J-R, Kim K-S, Manukyan KV, Mukasyan AS. Combustion synthesis of zero-, one-, two- and three-dimensional nanostructures: current trends and future perspectives. Prog Energy Combust Sci 2017;63:79–118.

[2] Mukasyan AS, Rogachev AS, Aruna ST. Combustion synthesis in nanostructured reactive systems. Adv Powder Technol 2015;26:954–76.

[3] Aruna ST, Mukasyan AS. Combustion synthesis and nanomaterials. Curr Opin Solid State Mater Sci 2008;12:44–50.

[4] Xin-Wei Zhang, Zheng-He Hua, Yu-Wen Jiang, Shao-Guang Yang. Progress in sol-gel autocombustion synthesis of metals and alloys. Acta Phys Sin 2015;64, 98101-098101.

[5] Varma A, Mukasyan AS, Rogachev AS, Manukyan KV. Solution combustion synthesis of nanoscale materials. Chem Rev 2016;116:14493–586.

[6] Wen W, Wu J-M. Nanomaterials via solution combustion synthesis: a step nearer to controllability. RSC Adv 2014;4:58090–100.

[7] Li F-t, Ran J, Jaroniec M, Qiao SZ. Solution combustion synthesis of metal oxide nanomaterials for energy storage and conversion. Nanoscale 2015;7:17590–610.

[8] Deganello F, Tyagi AK. Solution combustion synthesis, energy and environment: best parameters for better materials. Prog Cryst Growth Charact Mater 2018;64:23–61.

[9] Thoda O, Xanthopoulou G, Vekinis G, Chroneos A. Review of recent studies on solution combustion synthesis of nanostructured catalysts. Adv Eng Mater 2018;20:1800047.

[10] Specchia S, Ercolino G, Karimi S, Italiano C, Vita A. Solution combustion synthesis for preparation of structured catalysts: a mini-review on process intensification for energy applications and pollution control. Int J Self-Propag High-Temp Synth 2017;26:166–86.

[11] Pourgolmohammad B, Masoudpanah SM, Aboutalebi MR. Effects of the fuel type and fuel content on the specific surface area and magnetic properties of solution combusted CoFe2O4 nanoparticles. Ceram Int 2017;43:8262–8.

[12] Manukyan KV, Chen Y-S, Rouvimov S, Li P, Li X, Dong S, et al. Ultrasmall α-Fe2O3 superparamagnetic nanoparticles with high magnetization prepared by template-assisted combustion process. J Phys Chem C 2014;118:16264–71.

[13] Gu Y, Qin M, Cao Z, Jia B, Wang X, Qu X. Effect of glucose on the synthesis of Iron carbide nanoparticles from combustion synthesis precursors. J Am Ceram Soc 2016;99:1443–8.

[14] Chen W, Li F, Yu J, Liu L. A facile and novel route to high surface area ceria-based nanopowders by salt-assisted solution combustion synthesis. Mater Sci Eng B 2006;133:151–6.

[15] Pourgolmohammad B, Masoudpanah SM, Aboutalebi MR. Effect of starting solution acidity on the characteristics of CoFe2O4 powders prepared by solution combustion synthesis. J Magn Magn Mater 2017;424:352–8.

[16] Naveenkumar A, Kuruva P, Shivakumara C, Srilakshmi C. Mixture of fuels approach for the synthesis of SrFeO3−δ nanocatalyst and its impact on the catalytic reduction of nitrobenzene. Inorg Chem 2014;53:12178–85.

[17] Ianos R, Istratie R, Pacurariu C, Lazau R. Solution combustion synthesis of strontium aluminate, SrAl2O4, powders: single-fuel versus fuel-mixture approach. PCCP 2016;18:1150–7.

[18] Jiang S, Hu T, Gild J, Zhou N, Nie J, Qin M, et al. A new class of high-entropy perovskite oxides. Scripta Mater 2018;142:116–20.

[19] Dąbrowa J, Stygar M, Mikuła A, Knapik A, Mroczka K, Tejchman W, et al. Synthesis and microstructure of the (Co,Cr,Fe,Mn,Ni)3O4 high entropy oxide characterized by spinel structure. Mater Lett 2018;216:32–6.

[20] Nagarajan V, Thayumanavan A. MgFe2O4 thin films for detection of ethanol and acetone vapours. Surf Eng 2018;34:711–20.

[21] Polat K, Yurdakoc M. Solar decolorization of methylene blue by magnetic MgFe2O4-MWCNT/Ag3VO4 visible active photocatalyst. Water Air Soil Pollut 2018;229:331.

[22] Henning RA, Uredat P, Simon C, Bloesser A, Cop P, Elm MT, et al. Characterization of MFe2O4 (M = Mg, Zn) thin films prepared by pulsed laser deposition for photoelectrochemical applications. J Phys Chem C 2019;123:18240–7.

[23] Joulaei M, Hedayati K, Ghanbari D. Investigation of magnetic, mechanical and flame retardant properties of polymeric nanocomposites: green synthesis of MgFe2O4 by lime and orange extracts. Compos Part B Eng 2019;176:107345.

[24] Jia J, Du X, Zhang Q, Liu E, Fan J. Z-scheme MgFe2O4/Bi2MoO6 heterojunction photocatalyst with enhanced visible light photocatalytic activity for malachite green removal. Appl Surf Sci 2019;492:527–39.

[25] Yu S, Sun C-J, Chow G-M. 1 - chemical synthesis of nanostructured particles and films A2 - Koch, Carl C, nanostructured materials (Second edition). Norwich, NY: William Andrew Publishing; 2007. p. 3–46.

[26] Johnson JD, Bell NJ, Donahoe EL, Macfarlane RD. Metal ion complexes of EDTA as solutes for density gradient ultracentrifugation: influence of metal ions. Anal Chem 2005;77:7054–61.
[27] Zabiszak M, Nowak M, Taras-Goslinska K, Kaczmarek MT, Hnatejko Z, Jastrzab R. Carboxyl groups of citric acid in the process of complex formation with bivalent and trivalent metal ions in biological systems. J Inorg Biochem 2018;182:37–47.
[28] Hoyau S, Pélicier J-P, Rogalewicz F, Hoppilliard Y, Ohanessian G. Complexation of Glycine by atomic metal cations in the gas phase. Eur J Mass Spectrom (Chichester) 2001;7: 303–11.
[29] Gutten O, Rulíšek L. Predicting the stability constants of metal-ion complexes from first principles. Inorg Chem 2013;52:10347–55.
[30] Wacker M, Seubert A. Determination of stability constants of strong metal–ligand complexes using anion or cation exchange chromatography and atomic spectrometry detection. J Anal At Spectrom 2014;29:707–14.
[31] Erri P, Pranda P, Varma A. Oxidizer—Fuel interactions in aqueous combustion synthesis. 1. Iron(III) nitrate—Model fuels. Ind Eng Chem Res 2004;43:3092–6.
[32] Goldman A. Modem ferrite technology. 2 ed. Pittsburgh, PA, USA: Springer; 2006.
[33] Cobos MA, de la Presa P, Llorente I, Alonso JM, García-Escorial A, Marín P, et al. Magnetic phase diagram of nanostructured zinc ferrite as a function of inversion degree δ. J Phys Chem C 2019;123:17472–82.
[34] Somnath, Sharma I, Kotnala RK, Singh M, Kumar A, Dhiman P, et al. Structural, magnetic and Mössbauer studies of Nd-doped Mg-Mn ferrite nanoparticles. J Magn Magn Mater 2017;444:77–86.
[35] Sharma R, Thakur P, Kumar M, Barman PB, Sharma P, Sharma V. Enhancement in A-B super-exchange interaction with Mn2+ substitution in Mg-Zn ferrites as a heating source in hyperthermia applications. Ceram Int 2017;43:13661–9.
[36] Kumar G, Kotnala RK, Shah J, Kumar V, Kumar A, Dhiman P, et al. Cation distribution: a key to ascertain the magnetic interactions in a cobalt substituted Mg–Mn nanoferrite matrix. PCCP 2017;19:16669–80.
[37] Chen R, Christiansen MG, Anikeeva P. Maximizing hysteretic losses in magnetic ferrite nanoparticles via model-driven synthesis and materials optimization. ACS Nano 2013;7:8990–9000.
[38] Lee J-H, Jang J-t, Choi J-s, Moon SH, Noh S-h, Kim J-w, et al. Exchange-coupled magnetic nanoparticles for efficient heat induction. Nat Nano 2011;6:418–22.
[39] Sing KSW, Everett DH, Haul RAW, Moscou L, Pierotti RA, Rouquerol J, et al. Reporting physisorption data for Gas/Solid systems. In: Handbook of heterogeneous catalysis. Wiley-VCH Verlag GmbH & Co. KGaA; 2008.
[40] Zaki HM, Al-Heniti S, Al Shehri N. New scheme for cation distribution and electrical characterization of nanocrystalline aluminum doped magnesium ferrite MgAlxFe2−xO4. Physica B Condens Matter 2014;436:157–63.
[41] Sickafus KE, Wills JM, Grimes NW. Structure of spinel. J Am Ceram Soc 1999;82:3279–92.
[42] Spaldin NA. Magnetic materials: fundamentals and applications. Cambridge University Press; 2010.
[43] Cullity BD, Graham CD. Introduction to magnetic materials. New Jersay: John Wiley & Sons; 2011.
[44] Lazarova T, Kovacheva D, Georgieva M, Tzankov D, Tyuliev G, Spassova I, et al. Tunable nanosized spinel manganese ferrites synthesized by solution combustion method. Appl Surf Sci 2019;496:143571.